Front. Phys.
https://doi.org/10.15302/frontphys.2027.056202

CN 11-5994/O4
ISSN 2095-0462

RESEARCH ARTICLE

Conceptual Feasibility of Space Power Station with Pulsed and Unconfined Fusion

Yanglin Hu(胡杨林)*[1,2], Yu Shi(施郁)†[3,4] and Biao Wu(吴飙)‡[5,3,6,7]

[1] *Centre for Quantum Technologies, National University of Singapore, Singapore*

[2] *QICI Quantum Information and Computation Initiative, School of Computing and Data Science, The University of Hong Kong, Pokfulam Road, Hong Kong SAR, China*

[3] *Wilczek Quantum Center, Shanghai Institute for Advanced Studies, University of Science and Technology of China, Shanghai 201315, China*

[4] *University of Science and Technology of China, Hefei 230026, China*

[5] *International Center for Quantum Materials, Peking University, 100871, Beijing, China*

[6] *Hefei National Laboratory, Hefei 230088, China*

[7] *Beijing Key Laboratory of Quantum Devices, Peking University, Beijing 100871, China*

Received July 29, 2026; accepted November 19, 2026

Just Accepted

This is a “Just Accepted” manuscript, which has been examined by the peer-review process and has been accepted for publication. A “Just Accepted” manuscript is published online shortly after its acceptance, which is prior to technical editing and formatting and author proofing. Higher Education Press (HEP) provides “Just Accepted” as an optional and free service which allows authors to make their results available to the research community as soon as possible after acceptance. After a manuscript has been technically edited and formatted, it will be removed from the “Just Accepted” Web site and published as an Online First article. Please note that technical editing may introduce minor changes to the manuscript text and/or graphics which may affect the content, and all legal disclaimers that apply to the journal pertain. In no event shall HEP be held responsible for errors or consequences arising from the use of any information contained in these “Just Accepted” manuscripts. To cite this manuscript please use its Digital Object Identifier (DOI®), which is identical for all formats of publication.

*yanglin.hu@u.nus.edu
†yu_shi@ustc.edu.cn
‡wubiao@pku.edu.cn

Conceptual Feasibility of Space Power Station with Pulsed and Unconfined Fusion

Abstract

Nuclear fusion offers the highest energy output per unit mass, making it attractive as an energy resource, in particular for space missions with severe payload constraints. The central challenge for terrestrial fusion is how to achieve high fuel temperature, density, and confinement for a meaningful fraction of the fuel to burn. Here we propose a conceptual design for a space-based fusion reactor driven by pulsed and unconfined fusion events. We analyze the destructive effects of such reactions on the structure and show that at about radius 10^2 m, the reactor design can withstand them. The estimated net electric power output is about 1 GW. Our findings demonstrate that, under reasonable parameter assumptions, this reactor is plausible from physical standpoint, while challenging from engineering perspective. Among other usages, our fusion power station provides efficient energy to space-based computing, AI and data facilities. This conceptual design is worth further investigation as a potential pathway toward practical fusion power stations. Our results establish a preliminary theoretical possibility under order-of-magnitude assumptions. The detailed neutron-transport, structural-dynamics, and power-conversion analyses required to establish engineering feasibility are deferred to future research.

Keywords— Nuclear fusion, inertial confinement, space power station

1 Introduction

Energy has always been a cornerstone of human survival and progress. In the current era, information processing depends on energy, and the latest competition in artificial

intelligence has, to a large extent, become a competition over energy. We propose here a conceptual design of a space-based fusion power station, which may be the eventual energy source for future space activities. Indeed, space-based data centers and computing and AI facilities in near-Earth space have been proposed as a potential means to reduce power and cooling constraints on Earth [1]. For this purpose, the space-grade solar panels can achieve only a few hundreds $\mathrm{W\,kg^{-1}}$, 10 orders of magnitude less than the deuterium-tritium fusion reaction, which we propose for space activities. Furthermore, recent ground demonstrations for the Sun-Chasing Project [2,3] successfully achieved kilowatt-level, one-to-many microwave power transmission to moving targets over hundred-meter distances. This breakthrough validates the possibility that our space-based fusion station could effectively supply energy to simultaneous space and ground activities through electromagnetic waves.

Fusion promises high, continuous, distance-independent power in a compact form, and has long been considered as the ultimate energy source [4]. The solar energy originally comes from fusion reactions inside the Sun. Fusion reaction is the process in which two light atomic nuclei merge into a heavier nucleus, releasing a substantial amount of energy due to the increase in nuclear binding energy [5]. Fusion reactions release more energy per unit mass than chemical or fission reactions [6].

Such weight-efficient power sources are especially attractive for space missions, where payload mass is costly. In the 1950s and 1960s, Project Orion investigated spacecraft propelled directly by nuclear explosions [7–9]. For deep-space activities, such as interstellar travels, solar power becomes increasingly ineffective at large distances from the Sun, and weight-efficient and high-power fusion stations have been proposed as a possible solution [10–13].

Although thermonuclear devices have achieved enormous energy release via fusion [14], fusion has not yet been realized as a practical power source [15]. A central challenge for fusion is to make the fuel hot enough to reach the fusion energy threshold, dense enough to enhance the fusion reaction rate, and confined long enough to achieve significant burn-up [16]. In practice, there are also engineering constraints imposed by intense neutron

and heat fluxes on the fusion reactor container [17].

To overcome these challenges, two major approaches have been pursued. One is magnetic confinement, which uses strong magnetic fields to confine the high-temperature fuel for controlled fusion reactions [18]. However, this approach remains out of reach due to limitations in magnet technology, plasma instabilities, radiation damage, and other factors [17, 19–21]. The other approach is inertial confinement, in which the fuel is rapidly compressed and heated such that a significant portion undergoes fusion within a few nanoseconds before the fuel disassembles [22]. Laser-driven inertial confinement achieves compression via intense laser pulses, but suffers from low energy efficiency, high repetition rate requirements, and difficult target fabrication, among other issues [23]. Thermonuclear devices are also based on inertial confinement, with compression and heating of the fusion fuel achieved by a fission stage followed by pulsed and unconfined fusion reactions. These devices release enormous energy through blast and thermal effects instantaneously and destructively [14], which makes this type of fusion unsuitable for power generation on Earth. Recent advances have enabled the design of such devices to maximize the yield of either neutrons, as neutron bombs [24], or electromagnetic pulses, as EMP bombs [25], while reducing blast and thermal effects. It was suggested that fusion rates can be enhanced by various mechanisms [26], such as electrochemical loading [27] or plasmonic resonance [28, 29], potentially enabling low-energy fusion through alternative approaches. A detailed exploration of these mechanisms lies beyond the scope of the present work.

We present a conceptual framework for a space-based fusion energy system based on pulsed and unconfined fusion reactions. We have examined the underlying physics principles and engineering challenges of this approach. Our preliminary analysis indicates that such a system is conceptually feasible from physics point of view while requiring further development to overcome significant engineering challenges. Although early-stage development of our proposed design could facilitate nuclear disarmament, the mature architecture would transition toward fusion devices tailored exclusively for large-scale, peaceful energy generation.

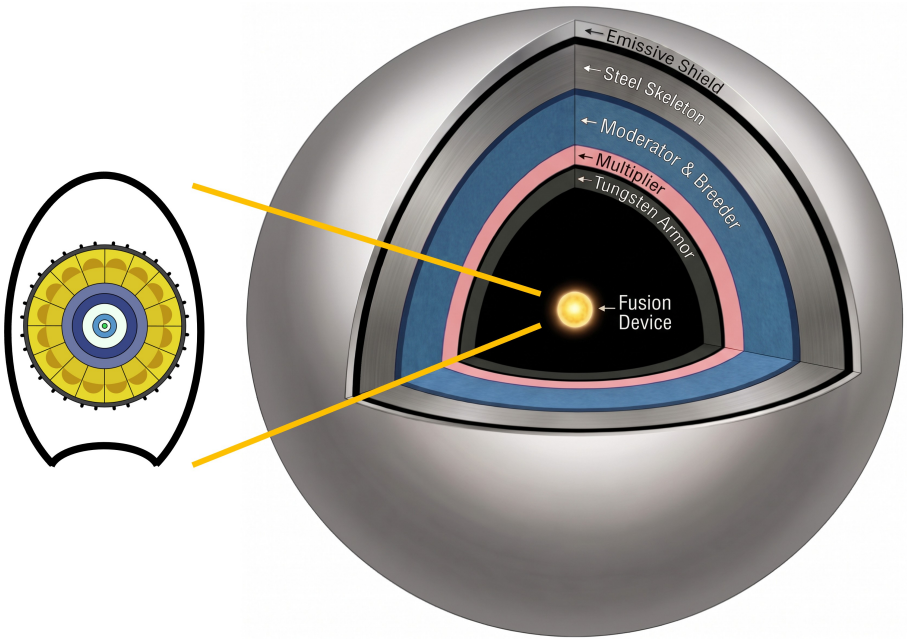


Figure 1: Conceptual design of the fusion reactor. The fusion device is placed at the center of the fusion blanket, possibly by a robot or a projectile. From the plasma-facing side to the outside, the blanket consists of a tungsten armor layer (inner black layer), a beryllium neutron multiplier layer (pink layer), a combined water moderator and lithium breeder layer (blue layer), a steel structural skeleton (gray layer), and an outer high-emissivity shield (outer silver layer). The radius of the central cavity is r, the thickness of the water and breeder layer is D, and that of the steel skeleton is H.

Our design resembles a Dyson sphere [30], but on a miniature scale and the star is replaced by fusion devices. There were conceptual proposals such as Project PACER [31–33] considering fusion power station with pulsed and unconfined fusion events deep underground, ceased due to cavity survival and seismic damage caused by destructive blast and thermal effects. The key insight underlying our proposal is that in the absence of a substantial atmosphere, such as at high altitude or in space, the energy of a pulsed and unconfined fusion event is released primarily via neutrons, alpha particles and gamma or X rays [14, 34]. This radiation is less destructive to the tungsten armor layer than blast, because neutrons transfer much less energy per collision to a heavy nucleus than to a light nucleus. Therefore, pulsed and unconfined fusion reactions may be more suitable for energy production in space-based fusion power stations.

2 Nuclear reaction

In this section, we analyze the key nuclear reactions relevant to a fusion power station, including both the primary reactions in fusion devices and the secondary reactions in the blanket.

We consider a fusion power station fueled by a device based on the deuterium-tritium (D-T) fusion reaction [24, 35, 36]

$$\mathrm{D} + \mathrm{T} \longrightarrow {}^4\mathrm{He} + \mathrm{n} + 17.6\,\mathrm{MeV}. \tag{1}$$

The D-T fusion cross section reaches its maximum at kinetic energy of approximately 64 keV in the center-of-mass frame, with a peak value of 5.0 b [36, 37]. For an order-of-magnitude estimate, we therefore assume that D-T fusion occur at a fixed kinetic energy of 64 keV in the center-of-mass frame. Since the released energy is 17.6 MeV, this initial energy to enable the fusion reaction affects the product energies only at the percent level.

The kinetic energies of the fusion products in the center-of-mass frame follow from energy and momentum conservations [36]

$$\begin{aligned} \frac{1}{2} m_\mathrm{n} v_\mathrm{n}^2 + \frac{1}{2} m_\alpha v_\alpha^2 &= 17.6\,\mathrm{MeV}, \\ m_\mathrm{n} \mathbf{v}_\mathrm{n} + m_\alpha \mathbf{v}_\alpha &= 0. \end{aligned} \tag{2}$$

where m_n and $\mathbf{v}_\mathrm{n}$ are the mass and the velocity of the neutron, m_α and $\mathbf{v}_\alpha$ are those of the alpha particle. One obtains

$$\begin{aligned} E_\mathrm{n} &= 14.1\,\mathrm{MeV}, \quad v_\mathrm{n} = 5.2 \times 10^7\,\mathrm{m\,s^{-1}}, \\ E_\alpha &= 3.5\,\mathrm{MeV}, \quad v_\alpha = 1.30 \times 10^7\,\mathrm{m\,s^{-1}}. \end{aligned} \tag{3}$$

These are the standard D-T fusion product energies. The small initial energy is neglected. We will use these values throughout the main text.

It is worth noting that the relativistic corrections to energy and momentum scale proportional to $\beta^2 = \frac{v^2}{c^2}$ and thus becomes significant only if β^2 approaches 1. For

neutrons $\beta_{\mathrm{n}}^2 \approx 3 \times 10^{-2}$ and alpha particles $\beta_{\alpha}^2 \approx 2 \times 10^{-3}$. Therefore, there is no need to take relativistic effects into account.

Here we treat the radiation field simply as non-relativistic 14.1 MeV neutrons and 3.5 MeV alpha particles, serving as a practical first-order approximation. A detailed engineering analysis of radiation transport is ultimately necessary. Specifically, neutron scattering, secondary gamma production, activation, and transient energy deposition are not modeled in the present analysis. Consequently, the calculations for radiation pressure and structural response later in this paper remain first-order estimates. A dedicated analysis of these factors will be required to properly assess their effects in future designs. Because the present work is a conceptual exploration of the feasibility of this space power station, we defer such an analysis to future work.

We now list a few more nuclear reactions that are needed in the analysis of our design.

A fusion reactor requires an armor layer made of tungsten to protect the first wall against high-energy charged particles, such as alpha particles and plasma debris. Consequently, it is necessary to account for the nuclear reactions between the incident fusion neutrons and the tungsten armor. In addition to elastic and inelastic scattering, an incoming fast neutron can knock out a bound neutron from the tungsten nucleus. Letting A denote the mass number of the relevant tungsten isotope, this $(n, 2n)$ reaction is given by

$$^{\mathrm{A}}\mathrm{W} + \mathrm{n(fast)} \longrightarrow {}^{\mathrm{A-1}}\mathrm{W} + 2\,\mathrm{n}. \tag{4}$$

The continuous operation of the fusion power station relies on a sustainable supply of fuel, namely deuterium and tritium. Deuterium is stable and can be stockpiled. In extreme scenarios, it can also be produced via neutron capture on hydrogen [38],

$$^{1}\mathrm{H} + \mathrm{n} \longrightarrow \mathrm{D} + 2.2\,\mathrm{MeV}. \tag{5}$$

Conversely, tritium is a radioactive isotope of hydrogen with a half-life of 12.3 years [39]. It cannot be stored forever and must be continuously bred in the long run to support extended missions, such as interstellar travel. A common approach is to breed tritium

with the lithium isotope ^{6}Li [36],

$$^6\mathrm{Li} + \mathrm{n(slow)} \longrightarrow {}^4\mathrm{He} + \mathrm{T} + 4.8\,\mathrm{MeV}. \tag{6}$$

As shown above, one tritium nucleus consumed in the fusion event generates one fusion neutron, and one neutron captured in the blanket breeds one tritium atom. In reality, however, the neutron economy inevitably suffers from geometric leakage and parasitic absorption. To establish a self-sustaining tritium fuel cycle, the fusion neutrons must be multiplied before they are captured. Neutron multipliers, such as beryllium, are therefore necessary to increase the neutron population via neutron multiplication reactions [38],

$$^9\mathrm{Be} + \mathrm{n(fast)} \longrightarrow {}^8\mathrm{Be} + 2\,\mathrm{n} - 1.57\,\mathrm{MeV}, \tag{7}$$

where the ^{8}Be ground state is unbound by 92 keV with respect to breakup into two alpha particles, and has a half-life on the order of 10^{-16} s [40].

We will utilize the reactions above for the reactor design and parameter estimates in the subsequent sections.

3 Reactor design

Our conceptual design for fusion reactor of pulsed and unconfined fusion reactions is illustrated in Fig. 1. It is broadly inspired by established fusion reactor with confined plasma, adapted to a space-based fusion reactor powered by pulsed and unconfined fusion reactions. We consider a spherical chamber whose inner wall serves as the blanket. Compact fusion devices are delivered to the center of the shell, either by robots operating between pulses or projectiles launched from a magazine, to start pulsed and unconfined fusion events. The fusion products deposit energy in the surrounding layered structure. From the radiation-facing side to the outside, the blanket consists of a tungsten armor layer, a beryllium multiplier layer, a combined lithium breeder and water moderator layer, a steel structural skeleton, and an outer high-emissivity radiator layer

(e.g., treated aluminum or carbon-carbon composites).

The tungsten armor layer protects the station against alpha particles and debris cloud generated by the pulsed and unconfined fusion reactions. The 3.5 MeV charged alpha particles from D-T fusion lose energy rapidly in solids by ionization and excitation. In tungsten, their penetration depth is roughly 6 μm [41, 42], so their energy is mainly deposited near the tungsten layer and conducted into the coolant. Neutrons, by contrast, are uncharged and penetrate much deeper. Moreover, neutrons only transfer a small fraction of their energy per collision in elastic collisions with heavy nuclei, meaning that tungsten is an inefficient moderator [43, 44]. Taking the density of tungsten as $1.93 \times 10^4\,\mathrm{kg\,m^{-3}}$, the mean free path of 14.1 MeV neutrons is 3.0 cm. To shield alpha particles and debris but let go neutrons, we thus take 1.00 cm as the typical thickness of the armor layer.

Right behind the tungsten armor layer is the multiplier layer consisting of beryllium ^{9}Be. The multiplier can increase the neutron population via the $(n, 2n)$ multiplication reaction. Taking the density of beryllium as $1.85 \times 10^3\,\mathrm{kg\,m^{-3}}$, the mean free path of 14.1 MeV neutrons is 5.4 cm. To ensure significant multiplication, we thus take 4.00 cm as the typical thickness of the multiplier layer.

Following the multiplier, a combined moderator and breeder layer consisting of water and lithium (^{6}Li) serves to moderate neutrons and breed tritium. The water gets heated up by cooling the structure and moderating the neutrons, which can then be used for energy production. As neutrons and protons are of nearly the same mass, surviving fast neutrons efficiently transfer their energy to protons through repeated elastic scattering on hydrogen. The 10 MeV charged recoil protons are quickly stopped in water by ionization and excitation within 1×10^{-2} m [45]. In water, the mean free path for collisions between 14.1 MeV neutrons and hydrogen atoms equals 15 cm [43, 44], and significant moderation down to thermal energies typically requires several decimeters to a few meters [46]. Therefore, we take 1.00 m as the typical thickness of this combined water and breeder layer. Once moderated by the water, as the thermal capture cross section of ^{6}Li is orders of magnitude larger than that of water or structural materials, the thermal neutrons are

dominantly captured by ^{6}Li to breed tritium. Furthermore, although water is not a perfect absorber of gamma and X-rays [47], this combined layer helps reduce any residual gamma and X-ray flux due to its extraordinary thickness.

Both the multiplier and breeder layers are necessary to ensure the fuel self-sufficiency and long-term operation of the fusion power station [43, 44].

The next layer, the steel structural skeleton, supports the mechanical pressure arising from the moderation and the absorption of neutrons and alpha particles.

Because the reactor operates in space, heat rejection relies entirely on blackbody radiation. To maximize the cooling power rate and thus overall electrical power output, the station requires an outer high-emissivity layer to efficiently shed excess heat. For simplicity, we will take emissivity $\epsilon = 0.9$ in our calculation. When constructed from suitable radiator materials, such as treated aluminum or carbon-carbon composites, this outer layer can simultaneously shield against cosmic rays such as protons and positrons that may affect the fusion reaction.

Given the intense and unavoidable cosmic ray bombardment in space, the material selection for a space-based D-T fusion blanket must prioritize radiation tolerance over terrestrial performance metrics. The tungsten armor layer requires alloying with rhenium (e.g., W−5Re) to mitigate neutron-induced embrittlement [48, 49].

As this study serves as a conceptual exploration, we select beryllium as the primary neutron multiplier and lithium as the tritium breeder for a simplified neutronic analysis. In practical reactor engineering, however, the selection of breeding and multiplying materials must also account for their mechanical, thermal, and chemical properties. Beryllium is an effective neutron multiplier because of its relatively low threshold energy for the neutron multiplication reaction and its low neutron absorption probability. ^{6}Li has a large capture cross section for low-energy neutrons. Moreover, the relatively light nuclei of beryllium and lithium can efficiently moderate high-energy fusion neutrons through elastic scattering. These properties make beryllium-lithium systems attractive candidates for achieving a high tritium breeding ratio [50, 51]. However, beryllium suffers from severe swelling, helium embrittlement, and pyrophoricity under cosmic ray exposure [52, 53],

and lithium also suffers its strong reactivity with water and air [54], which must be considered for an actual reactor. An alternative is the liquid lead–lithium eutectic alloy ($\mathrm{Li}-\mathrm{Pb}$) [50, 55]. The alloy offers reduced chemical reactivity. Furthermore, lead is susceptible to spallation from cosmic-ray protons, this effect can be intentionally harnessed, as each high-energy proton striking a lead nucleus generates a shower of 10–30 spallation neutrons that actively enhance tritium breeding beyond the fusion reactions themselves [56–58]. Nevertheless, lead introduces other limitations. The endothermic neutron multiplication reaction of lead consumes 7.4 MeV for $^{208}\mathrm{Pb}$ [51], depending strongly on the incident neutron energy spectrum. Besides, the high atomic mass of lead makes it an inefficient neutron moderator. Additional challenges include corrosion of structural materials, tritium permeation, and compatibility with the cooling system [59, 60]. Therefore, while lead–lithium remains a promising alternative for practical reactors, we retain beryllium–lithium as a simplified model for our conceptual design.

Finally, the structural steel can be oxide dispersion-strengthened (ODS) steel, whose nanoscale oxide particles trap radiation-induced helium bubbles and prevent grain boundary embrittlement [61, 62].

4 Tritium breeding

We estimate the tritium breeding ratio for a simplified fusion reactor geometry. The setup consists of a $d_{\mathrm{W}} = 1\,\mathrm{cm}$ armor layer made of tungsten, a $d_{\mathrm{Be}} = 4\,\mathrm{cm}$ neutron multiplier layer made of beryllium and a thick enough neutron moderator and tritium breeder layer made of water and lithium.

In the estimate above, we specify the moderator to be water and the breeder to be lithium. The exact chemical form of the lithium is left unspecified because we assume the combined layer is sufficiently thick to fully moderate the fast neutrons, and the thermal capture cross section of $^{6}\mathrm{Li}$ (940 b) exceeds those of water (0.6 b), steel (2.6 b) or other elements to form a component by orders of magnitude. Consequently, we assume that thermal neutrons are dominantly captured by $^{6}\mathrm{Li}$ regardless of its specific chemical

compound, making our idealized model sufficient for a first-order neutronics estimate. Natural lithium contains only 7.5 % of ^{6}Li, so a practical breeding medium would require lithium enriched in ^{6}Li (typically 30% to 90%). This enrichment level dictates the necessary ^{6}Li number density for an operational reactor, the optimization of which is left to future detailed engineering designs. Finally, because elemental lithium is highly chemically reactive with the water moderator, a practical engineering design must utilize a lithium compound compatible with water, physically separate the two media, or adopt a combined moderator and breeder alternative. Standard candidates include the soluble lithium salt $LiNO_3$ compatible with the water moderator [63], solid lithium ceramics like Li_4SiO_4 in pebble bed form, the liquid lead–lithium eutectic Pb−17 Li, or molten salts such as $LiF-BeF_2$ [50,59]. Nevertheless, we retain the simplified water and lithium layers as our conceptual baseline to clearly illustrate the underlying moderation and breeding physics.

For the $d_W = 1\,\text{cm}$ armor layer made of tungsten, the cross section of tungsten for 14.1 MeV is approximately 5.4 b, consisting of 2.4 b elastic scattering with almost no energy change, 2.4 b $(n, 2n)$ neutron multiplication, and 0.5 b inelastic collision [38]. The mean free path of a neutron in tungsten is $\lambda_W \approx 3.0\,\text{cm}$. For an armor thickness of $d_W = 1\,\text{cm}$ sufficient to shield alpha particles and debris, the probability of a ballistic neutron is 71.7 %. For each incident neutron, 0.717 neutrons enters the multiplier layer without collision. The remaining 0.283 interact within the tungsten armor, among them 0.126 are elastic, 0.126 are multiplied and 0.026 are inelastic. Using the cross sections of all processes, each incident neutron produces 0.843 fast neutrons from ballistic transmission and elastic collision and 0.278 slow neutrons from neutron multiplication and inelastic collision.

In the $d_{Be} = 4\,\text{cm}$ multiplier layer consisting of beryllium, the 0.843 fast neutrons remain above the 1.85 MeV threshold for $(n, 2n)$ neutron multiplication. At 14.1 MeV, the total cross section of ^{9}Be is approximately 1.50 b, consisting of 0.98 b elastic scattering, 0.48 b $(n, 2n)$ neutron multiplication, and 0.03 b inelastic collision [38]. The mean free path of a fast neutron in beryllium is $\lambda_{Be} \approx 5.35\,\text{cm}$. Thus, for a thickness of $d_{Be} = 4\,\text{cm}$,

Table 1: Neutron balance per incident 14.1 MeV fusion neutron, for the layer sequence of $d_{\mathrm{W}} = 1\,\mathrm{cm}$ tungsten, $d_{\mathrm{Be}} = 4\,\mathrm{cm}$ beryllium, thick water and ^{6}Li layer. Cross sections are taken from [38] at the stated energies.

Layer	Channel	Cross section (b)	Neutrons out
W (1 cm)	ballistic	—	0.717 (fast)
	elastic	2.4	0.126 (fast)
	$(n, 2n)$	2.4	0.252 (slow)
	inelastic	0.5	0.026 (slow)
^{9}Be (4 cm)	ballistic (fast)	—	0.402 (fast)
	elastic (fast)	0.98	0.288 (fast)
	$(n, 2n)$ (fast)	0.48	0.282 (slow)
	inelastic (fast)	0.03	0.009 (slow)
	others (slow)	—	0.278 (slow)
H_2O + ^{6}Li (thick)	capture by ^{6}Li	940	TBR ≈ 1.259

the probability of a fast neutron passing through without collision is 47.7 %. Consequently, among the 0.843 entering fast neutrons, 0.402 pass through ballistically, leaving 0.441 neutrons to interact. Among the 0.441 fast neutrons interacting in this beryllium layer, 0.288 are elastic, 0.141 are multiplied, and 0.009 are inelastic. Thus, after this beryllium layer, each incident neutron yields 0.690 fast neutrons from ballistic transmission and elastic collision, and 0.569 slow neutrons (from beryllium $(n, 2n)$ multiplication, inelastic collision, and the previous tungsten armor).

Finally, for a thick enough moderator and breeder layer consisting of water and lithium, all these neutrons are moderated to thermal neutrons by water and then transform into tritium by lithium. For thermal neutrons at roughly 25 meV, the total cross section of ^{6}Li is approximately 941 b, consisting of 940 b (n, α)T tritium breeding, 0.7 b elastic scattering, and 0.04 b radiative capture [38]. Because this tritium breeding cross section 940 b is orders of magnitude larger than the thermal neutron capture cross sections of typical coolants like water (0.6 b) or structural materials like steel (2.6 b), ^{6}Li is overwhelmingly more efficient at capturing slow neutrons. Assuming that the neutrons in the water and breeder layer are dominantly captured by ^{6}Li, the estimated tritium breeding ratio is:

$$\mathrm{TBR} \approx 1.259. \tag{8}$$

We emphasize that Eq. (8) is a first-order estimate; therefore, demonstrating a robust

Table 2: Sensitivity of the Tritium Breeding Ratio (TBR) to the beryllium multiplier thickness d_{Be} and systematic variations in all evaluated cross sections. The baseline column (0%) uses the nominal parameters from Table 1, while the ±10% columns correspond to globally scaling all cross sections up or down by 10%. This simplified model only considers the first collision.

d_{Be} (cm)	Cross section variation		
	−10%	0%	+10%
2	1.186	1.202	1.218
4	1.241	1.259	1.276
6	1.280	1.298	1.314
8	1.308	1.325	1.340

safety margin is more important than the exact value. Engineering designs for self-sufficient fusion blankets typically require TBR $\gtrsim$ 1.05–1.15 to cover geometric leakage and structural absorption not modeled here. To test the robustness of our estimate, we varied the beryllium multiplier thickness d_{Be} and applied a systematic ±10% variation to all evaluated cross sections. As summarized in Table 2, the estimated TBR remains safely above the standard engineering threshold under all considered conditions. While our sensitivity analysis focuses on the neutron multiplication steps, the overall margin remains robust because the final capture step is highly efficient. We can safely assume ^{6}Li absorbs almost all available slow neutrons, as its massive thermal capture cross section (940 b) ensures very few are lost to water (0.6 b) or steel (2.6 b)

While fully validating this design requires a 3D Monte Carlo simulation with MCNP or OpenMC to assess energy-dependent, multi-group neutron transport in the actual spherical geometry, including neutron scattering, secondary gamma production, and geometric leakage, our simplified model successfully demonstrates a comfortable breeding margin. We defer these rigorous numerical transport calculations to future work.

5 Device particular

The central challenge for the fusion reactor of pulsed and unconfined fusion reactions is whether the reactor structure survives the extreme conditions produced by the pulsed and unconfined fusion events. The typical yield of such a pulsed and unconfined fusion

event is on the order of 10^3 tTNT [24, 35]. For estimation, we will take

$$E_{\text{tot}} = 1.00 \times 10^3 \,\text{tTNT} = 4.18 \times 10^{12} \,\text{J}. \tag{9}$$

The TNT-equivalent yield is a measure of the total energy released by the device, with $1\,\text{tTNT} = 4.184 \times 10^9\,\text{J}$ by definition. In space of high vacuum, the energy is released mainly via prompt radiation, i.e. neutrons, alpha particles and gamma rays [14, 34]. We therefore assume that the entire yield is converted into nuclear radiation and kinetic energy of the fusion products. For the damage analysis presented here, the prompt radiation and the debris cloud are considered. Using the total yield per time and the released energy per D-T fusion reaction, the number of D-T fusion reactions per time is

$$N_{\text{tot}} = \frac{E_{\text{tot}}}{17.6\,\text{MeV}} \approx 1.48 \times 10^{24}. \tag{10}$$

In a realistic device, however, only a fraction of this energy originates from D–T fusion, while the remainder is released by the fission primary (and possibly by fission reactions in the surrounding materials). We therefore introduce the fusion fraction

$$E_{\text{fus}} = f_{\text{fus}} E_{\text{tot}}, \tag{11}$$

where E_{fus} corresponds to the energy released by fusion reactions while E_{tot} corresponds to the energy released by all reactions. We can thus write the neutron source strength per event as

$$N_{\text{n}} = f_{\text{fus}} N_{\text{tot}}, \tag{12}$$

Therefore, E_{tot} and N_{tot} in Eqs. (9) and (10) corresponds to the $f_{\text{fus}} = 1$ case where all energy and neutrons are contributed by fusion reactions. Throughout this paper, we assume a baseline fusion fraction $f_{\text{fus}} = 1$. All neutron-derived quantities, including the tritium breeding ratio TBR, the neutron pulse pressure p_n and the structural force F_n, scale linearly with f_{fus} and can be re-scaled accordingly for any other device design. We note that devices tailored for energy generation would be optimized toward high f_{fus},

which simultaneously minimizes fission-product residuals. A reduced f_{fus} would lower the neutron radiation load and hence relax the structural requirements derived below, so the f_{fus} assumption is conservative for the structural analysis.

Each time the fusion event produces two distinct radiation fronts that travel outward from the reaction point, including a faster neutron pulse which gets moderated and absorbed via scattering by the moderator and breeder layer and a slower alpha-particle pulse which gets stopped via ionization and excitation by the tungsten armor. These radiation pulses not only heat up the reactor but also impose mechanical force on its structure. Both effects are analyzed quantitatively in the following sections.

6 Power Generation

The energy released per fusion event, $E_{\mathrm{tot}} = 4.18 \times 10^{12}\,\mathrm{J}$, heats the spherical water shell of the fusion reactor with radius r and fixed thickness $D = 1.00\,\mathrm{m}$. The system operates as a supercritical water reactor [64], wherein the pressurized water is heated beyond its critical point to a hot bath temperature of $T_{\mathrm{hot}} = 773\,\mathrm{K}$. For space power stations, the heat rejection is governed by the blackbody radiation. Consequently, the maximum electrical power output is achieved when the temperature of the cold bath satisfies $T_{\mathrm{cold}} = 0.75 T_{\mathrm{hot}} \approx 580\,\mathrm{K}$ [65], yielding an ideal Carnot efficiency of $\eta = 25\,\%$.

We stress that the condition $T_{\mathrm{cold}} = 0.75 T_{\mathrm{hot}}$ does not correspond to the zero-power Carnot limit. Rather, it follows from maximizing the electric power output of an endoreversible heat engine. In this model, the internal cycle is reversible, and we set

$$\eta = 1 - \frac{T_{\mathrm{cold}}}{T_{\mathrm{hot}}}. \tag{13}$$

The irreversibility stems from the finite-rate heat exchange with the reservoirs—specifically, the input heating power due to neutron moderation and the output cooling power due to blackbody radiation.

To maintain the temperature gradient, the system must reject the excess heat via black-body radiation from the cold bath. By setting the emissivity $\epsilon = 0.9$ of the outer

radiating surface, the cooling power must balance the excess heat production rate. This imposes a constraint on the fusion event frequency f_{gen}:

$$\epsilon\sigma T_{\text{cold}}^4(4\pi r^2) = (1-\eta) f_{\text{gen}} E_{\text{tot}}, \tag{14}$$

where σ is the Stefan-Boltzmann constant. Therefore, the operating frequency is determined directly by the cooling power and the total energy per event:

$$f_{\text{gen}} = \frac{\epsilon\sigma T_{\text{cold}}^4(4\pi r^2)}{(1-\eta)E_{\text{tot}}}. \tag{15}$$

With the frequency fixed by heat rejection, the electrical power output W_{gen} emerges as a function of the radius r of the reactor and the surface emissivity ϵ:

$$W_{\text{gen}} = \eta f_{\text{gen}} E_{\text{tot}} = \frac{\eta}{1-\eta}\epsilon\sigma T_{\text{cold}}^4(4\pi r^2). \tag{16}$$

We will calculate the electric power output once we determine the radius of the fusion station.

Substituting Eq. (13) into Eq. (16) reveals that $W_{\text{gen}} \propto T_{\text{hot}} T_{\text{cold}}^3 - T_{\text{cold}}^4$. The mathematical maximum of this power output occurs at $T_{\text{cold}} = 0.75 T_{\text{hot}}$. This represents a maximum-power condition in the spirit of finite-time thermodynamics [66], adapted to radiative heat transfer in our case rather than linear heat transfer in [66]. Consequently, our adopted efficiency is a robust, finite-rate result evaluated at maximum power, rather than an unrealistic zero-power upper bound.

Our analysis here describes the thermodynamic conversion step only. A complete power-conversion chain incurs additional, multiplicative losses: turbine and generator efficiencies, finite temperature differences in the heat exchangers, the view factor and long-term surface degradation of the radiator, and the pumping power of the cooling loop. Taking component efficiencies of 90% for the turbine, 80% for the compressor, and 92% for the alternator, and 95% for the recuperator [67], the net electric power is expected to reach 63% of the idealized estimate in Eq. (16). Accordingly, the electric

power outputs in Sec. 9 acquires an additional factor 63% after derating. However, the conclusion that the station operates in the gigawatt class is unchanged.

7 Pulse duration

The mechanical force imposed on the reactor structure by nuclear radiation arises from microscopic collisions between radiation particles and atoms in the reactor materials. The radiation consists of two distinct pulses, a neutron pulse and an alpha-particle pulse, which are treated separately in the analysis below.

For a fixed fusion yield, the magnitude of the mechanical force imposed on the reactor is inversely proportional to the duration of the radiation pulse at the blanket surface. This pulse duration is governed by two independent factors, the initial pulse width Δt_{ini} which is the time interval over which the fusion reactions occur in the pulsed and unconfined fusion event and the additional propagation induced broadening $\Delta t_{\mathrm{add}}(r)$ which is the spreading arising from the velocity dispersion of the emitted particles during their flight over a distance r.

The initial pulse width is determined by the rate of the fusion reactions, which depends on the device design (e.g., tamper configuration, neutron reflector, and compression geometry). In a pulsed and unconfined fusion event, the nuclear reaction phase is extremely short, typically on the order of $10^{-9}\,\mathrm{s}$ [14,68,69]. As a toy model, we assume that all neutrons and alpha particles are released uniformly within this initial pulse interval, giving

$$\Delta t_{\mathrm{ini}} = 1.00 \times 10^{-9}\,\mathrm{s}. \tag{17}$$

The fusion reaction occurs when the fuel is heated to a temperature of the order of $10^{8}\,\mathrm{K}$, taken as $T = 1 \times 10^{8}\,\mathrm{K}$ for simplicity. The reacting deuterium and tritium ions possess thermal motions. Consequently, the velocity of the center of mass point of each reacting pair follows the Maxwell-Boltzmann distribution at temperature T. This thermal motion broadens the lab-frame velocity distribution of the fusion products. A convenient estimate of the velocity spread is the root-mean-square velocity of the center

of mass point:

$$\Delta v = \sqrt{\frac{3k_B T}{m_{\mathrm{D}} + m_{\mathrm{T}}}} = 7.1 \times 10^5\,\mathrm{m\,s^{-1}}. \tag{18}$$

After traversing a distance r, the difference in arrival time between the slowest and fastest particles of a given fusion product leads to an additional pulse interval, given approximately by

$$\Delta t_{\mathrm{add}}(r) = \frac{r}{v - \Delta v} - \frac{r}{v + \Delta v} \approx \frac{2r\Delta v}{v^2}, \tag{19}$$

for $\Delta v \ll v$. Using v_{n} and v_α for 14.1 MeV neutrons and 3.5 MeV alpha particles, respectively, we obtain

$$\begin{aligned} \Delta t_{\mathrm{add,n}}(r) &\approx r \cdot 5.2 \times 10^{-10}\,\mathrm{s\,m^{-1}}, \\ \Delta t_{\mathrm{add},\alpha}(r) &\approx r \cdot 8.3 \times 10^{-9}\,\mathrm{s\,m^{-1}}, \end{aligned} \tag{20}$$

where r is the radius of the blanket expressed in meters.

As an order-of-magnitude estimate, the total pulse width at the blanket is taken as the sum of the initial and propagation-induced contributions:

$$\Delta t(r) = \Delta t_{\mathrm{ini}} + \Delta t_{\mathrm{add}}(r). \tag{21}$$

A simple comparison shows that $\Delta t_{\mathrm{ini}} \ll \Delta t_{\mathrm{add}}(r)$ for $r \gtrsim 100\,\mathrm{m}$, whereas $\Delta t_{\mathrm{ini}} \gg \Delta t_{\mathrm{add}}(r)$ for $r \lesssim 1\,\mathrm{cm}$. As will be shown later, the reactor radius of interest lie in the regime $r \gtrsim 100\,\mathrm{m}$, where the additional propagation induced broadening dominates the pulse duration.

Finally, we estimate the pulse duration of the debris cloud. The debris cloud is formed from the vaporized structural materials of the device, which we model as a mass $M_{\mathrm{Ti}} = 100\,\mathrm{kg}$ of titanium. Assuming the debris absorbs a typical fraction $\xi_{\mathrm{Ti}} = 0.2$ of the total yield $4.18 \times 10^{12}\,\mathrm{J}$ [70, 71], the energy of the debris is $E_{\mathrm{Ti}} = 8.36 \times 10^{11}\,\mathrm{J}$. The mean expansion velocity is therefore:

$$v_{\mathrm{Ti}} = \sqrt{\frac{2E_{\mathrm{Ti}}}{M_{\mathrm{Ti}}}} = 1.29 \times 10^5\,\mathrm{m\,s^{-1}}. \tag{22}$$

To estimate the velocity spread of the expanding debris, we assume that the ab-

sorbed energy initially thermalizes the structural materials into a superheated plasma. By matching the absorbed energy E_{Ti} to the thermal energy of the vaporized titanium, we obtain

$$T = \frac{2m_{\mathrm{Ti}}E_{\mathrm{Ti}}}{3k_B M_{\mathrm{Ti}}} \approx 3.21 \times 10^7\,\mathrm{K}, \tag{23}$$

where M_{Ti} is the total mass of the titanium and m_{Ti} is the atomic mass of a single titanium atom.

The thermal motion of the titanium ions broadens the velocity distribution of the expanding debris. We estimate this velocity spread using the standard deviation of the absolute velocity for a Maxwell-Boltzmann distribution:

$$\Delta v_{\mathrm{Ti}} = \sqrt{\langle v^2\rangle - \langle v\rangle^2} = \sqrt{1 - \frac{8}{3\pi}}\, v_{\mathrm{Ti}} \approx 5.02 \times 10^4\,\mathrm{m\,s^{-1}}. \tag{24}$$

The pulse duration at distance r is:

$$\Delta t_{\mathrm{add,Ti}}(r) = \frac{r}{v_{\mathrm{Ti}} - \Delta v_{\mathrm{Ti}}} - \frac{r}{v_{\mathrm{Ti}} + \Delta v_{\mathrm{Ti}}} \approx r \cdot 7.08 \times 10^{-6}\,\mathrm{s\,m^{-1}}. \tag{25}$$

Comparing this to that of the neutrons, the debris pulse width broadens significantly greater than the neutron pulse width.

8 Force analysis

We now estimate the mechanical pressure imposed on the fusion reactor by the neutron and alpha-particle pulses. Recall from the previous section that each pulsed and unconfined fusion event produces N_{tot} neutrons and an equal number of alpha particles, with velocity v_{n} and v_α, respectively. The pulse duration at the blanket radius r is dominated by additional propagation induced broadening in Eq. (20) for $r \gtrsim 100\,\mathrm{m}$.

The mechanical pressure imposed by a given fusion product arises from the transfer of its momentum to the blanket. Assuming that all incident particles transfer their entire

momentum to the reactor, the time-averaged pressure over the pulse duration is

$$p(r) = \frac{N_{\text{tot}} m v}{4\pi r^2 \Delta t(r)}, \tag{26}$$

where $A = 4\pi r^2$ is the area of the interior surface of the blanket. Substituting velocities in Eq. (3) yields

$$\begin{aligned} p_{\text{n}}(r) &\approx \frac{1}{r^3} \cdot 1.96 \times 10^{13}\,\text{J}, \\ p_{\alpha}(r) &\approx \frac{1}{r^3} \cdot 1.22 \times 10^{12}\,\text{J}, \end{aligned} \tag{27}$$

when the blanket radius r is of 10^2 m. The contribution from neutron surpasses that from alpha particles. Furthermore, neutrons arrive earlier than alpha particles. Therefore, we focus on the neutron-induced pressure subsequently. The corresponding total mechanical force on the blanket is

$$F_{\text{n}} = p_{\text{n}}(r)\pi r^2 = \frac{1}{r} \cdot 6.15 \times 10^{13}\,\text{J}. \tag{28}$$

Eqs. (27) and (28) show that both pressure and force decrease rapidly with increasing blanket radius, central to the structural design discussed later.

We also present an order-of-magnitude estimation on the force of the debris cloud on the structure. Assuming that the debris cloud transfers its momentum to the armor layer uniformly within the pulse width, the mechanical pressure of the debris pulse is:

$$p_{\text{Ti}}(r) \approx \frac{1}{r^3} \cdot 1.45 \times 10^{11}\,\text{J}. \tag{29}$$

By comparing the pressure caused by the debris pulse and the neutron pulse, we see that $p_{\text{n}}(r) \gg p_{\text{Ti}}(r)$ and thus $F_{\text{n}} \gg F_{\text{Ti}}$.

The force calculations on the structure provided herein serve solely as order-of-magnitude estimates to establish baseline physical feasibility. The dynamic loads generated by a nanosecond-scale fusion pulse fall beyond the scope of this initial study. Specifically, our models do not consider stress-wave propagation, local plastic deformation, thermal stress, fatigue, or potential joint failure in the macro-structure. As such, the force should be interpreted cautiously as a first-order approximation. Before this force can be treated

as a reliable engineering parameter, future development must perform rigorous dynamic structural simulations to account for those complex mechanical responses.

The force estimates above are static equivalents. In the following, we now estimate the influence of the dynamic aspects of pulsed energy deposition by orders of magnitude.

At the radii of interest, the neutron pulse duration is dominated by propagation broadening, yielding $\Delta t_{\mathrm{n}} \approx 50\,\mathrm{ns}$ at $r \approx 100\,\mathrm{m}$ according to Eq. (20). On the contrary, the sound speed of steel is approximately $c_{\mathrm{steel}} \approx 5 \times 10^{3}\,\mathrm{m\,s^{-1}}$ [72], and thus the acoustic transit time across the $H = 1\,\mathrm{m}$ steel skeleton is approximately $\Delta t_{\mathrm{c}} = H/c_{\mathrm{steel}} \approx 0.2\,\mathrm{ms}$. Because the pulse duration is orders of magnitude shorter than the acoustic response time, the structure operates in the impulsive regime. The inertia of the structure prevents it from fully deforming under the instantaneous peak pressure of the pulse. Consequently, the dynamic nature of the energy deposition mitigates bulk material stresses. Applying the pulsed pressure as a quasi-static load, as evaluated in our preceding analysis, therefore represents a conservative upper bound for structural integrity.

Radiation possibly imposes ablation of the armor surface. The alpha particles carry a fraction of approximately 20% of the yield, or $8.37 \times 10^{11}\,\mathrm{J}$ per event, and deposit it within the $6\,\mu\mathrm{m}$ range in tungsten [41, 42]. Taking the alpha particle pulse duration as $\Delta t_{\alpha} \approx 100\,\mathrm{ns}$ and the thermal diffusivity of tungsten as $\kappa_{\mathrm{W}} = 6.93 \times 10^{-5}\,\mathrm{m^2/s}$ [73], the thermal diffusion length of tungsten during the pulse is $d_{\mathrm{heat}} = \sqrt{\kappa_{\mathrm{W}} \Delta t_{\alpha}} \approx 2.63\,\mu\mathrm{m}$ [74]. Therefore, surface ablation is expected as deposited energy cannot be conducted away within the pulse. The corresponding alpha-particle energy fluence is $6.66 \times 10^{6}\,\mathrm{J/m^2}$ at $r \approx 100\,\mathrm{m}$, which, compared to $5.66 \times 10^{6}\,\mathrm{J\,kg^{-1}}$ required to vaporize solid tungsten [73], corresponds to an ablated equivalent depth of order $60\,\mu\mathrm{m}$ per event in the worst case of complete local thermalization. Ablation is therefore the most severe surface effect of the design and motivates mitigation strategies such as enlarging the cavity radius or a replaceable armor layer. The debris cloud, although mechanically negligible, deposits its energy in the same armor layer and must be included in a detailed ablation model.

The neutrons carry a fraction of of approximately 80% of the yield, or $3.35 \times 10^{12}\,\mathrm{J}$ per event, and deposit it within the 1 m range in the water. The corresponding neutron

energy fluence is $2.67 \times 10^7\,\mathrm{J/m^2}$ at $r \approx 100\,\mathrm{m}$, leading to a temperature increase of 6.39 K. Therefore, the water layer and the steel skeleton remains far below their thermomechanical limits. The energy deposited does not lead to bulk structural failure.

The event frequency is fixed by Eq. (15), which evaluates to $f_{\mathrm{gen}} \approx 2.3 \times 10^{-4}\,\mathrm{Hz} \times 10^{-4}$ at $r \approx 100\,\mathrm{m}$. Over its 30-year operational life, the structure will undergo approximately 2.2×10^5 fusion pulses. This high number of fusion events places the structural skeleton in the high-cycle fatigue regime, where long-term degradation accumulates in elastic deformations. Concurrently, high-energy neutrons also alters the thermomechanical properties of the armor layer at 0.017 displacement per atom per full power year at $6.2\,\mathrm{kW/m^2}$ using values in [75], leading to a low level of embrittlement and transmutation. The required maintenance and replacement schedule for the station will be dictated by two competing material limits, i.e. the mechanical fatigue life of the skeleton under repeated pressure impulses and the cumulative radiation damage to the armor under high energy neutrons. These considerations reinforce the choice of radiation-tolerant materials such as W−5 Re armor and ODS steel skeleton discussed in Sec. 3 and motivate a replaceable panel architecture such as the Bucky ball geodesic frame discussed later.

9 Skeleton Construction

The fusion reactor, especially the steel structural skeleton, must withstand the imposed mechanical pressure generated by each pulsed and unconfined fusion event. This requires that the maximum stress in the steel structural skeleton remains below its tensile yield strength. For both designs considered here, the structural skeleton is assumed to be fabricated from a high-quality armor steel with a tensile yield strength of [76]

$$\sigma_{\mathrm{steel}} = 1.60 \times 10^9\,\mathrm{Pa}. \tag{30}$$

The shear yield strength is taken to be 0.6 times the tensile yield strength.

Two candidate skeleton configurations are analyzed and their minimum survivable radii are determined. Both are illustrated in Fig. 2. First, we consider a monolithic shell.

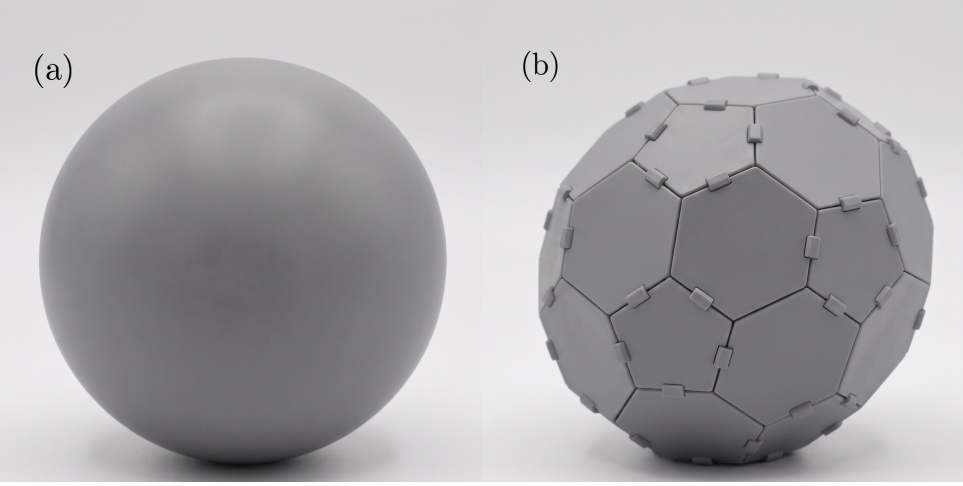


Figure 2: Two conceptual designs of the steel structural skeleton. (a) Monolithic shell. The steel structural skeleton is a solid spherical shell of uniform thickness 1.00 m. (b) Buckyball geodesic frame. The steel structural skeleton is tiled from a set of hexagonal and pentagonal steel panels. Each panel has side length of 7.5 m. Adjacent panels are joined along their edges by steel bars with cross-section of $1.00\,\mathrm{m}^2$, indicated by those rectangles connecting edges.

This design consists of a solid spherical shell of radius 78 m and uniform thickness 1.00 m as in Fig. 2(a). While theoretically optimal from a structural perspective, it presents substantial manufacturing challenges. The second design is a Buckyball geodesic frame of radius 2.1×10^2 m assembled from hexagonal and pentagonal steel panels, for example a Buckyball, each 1.00 m thick, with a side length of 7.5 m, see Fig. 2(b). Adjacent panels are joined along their edges by steel bars with a cross-section $1.00\,\mathrm{m}^2$. Although structurally less efficient than the monolithic shell, it is significantly more feasible to construct and maintain as panels could be manufactured on Earth and transported into space. We demonstrate below that both designs can safely withstand the imposed mechanical pressure produced by the neutron pulse from a 1.00×10^3 tTNT pulsed and unconfined fusion event in the following sections.

9.1 Design I: Monolithic Shell

Consider a solid spherical shell of radius r made of high-quality armor steel with a uniform wall thickness $H = 1.00\,\mathrm{m}$. This thickness is comparable to the turret armor of the Iowa-class battleships (495 mm) [77], highlighting that such choice is within the

realm of existing large-scale steel fabrication.

The pressure imposed on the inner surface of the reactor is 4.13×10^7 Pa for neutrons and 2.57×10^6 Pa for helium, respectively. These pressures are far less than the shear yield strength of the high-quality armor steel.

Furthermore, we use a simple strength model to estimate the tensile mechanical force on the shell. If the sphere is conceptually bisected along a great circle, the force required to separate the two hemispheres must be balanced by the stress in the cross-section. As $2\pi rH$ is the cross-sectional area of the cut, taking the yield in Eq. (30), the maximum tensile force that the shell can sustain is therefore

$$F_{\max,1} = \sigma_{\text{steel}} 2\pi r H = r \cdot 1.01 \times 10^{10}\,\text{Pa m}. \tag{31}$$

The mechanical force imposed on the blanket by the neutron pulse was derived in Eq. (28). Requiring that this tensile force not exceed the tensile capacity of the structure gives the condition for the structure to survive the neutron pulse

$$F_{\text{n}}(r) \leq F_{\max,1}(r) \quad \Longrightarrow \quad r \geq 78\,\text{m}. \tag{32}$$

A sphere of this radius is comparable in size to the Las Vegas Sphere, a famous spherical steel structure with a diameter of approximately 157 m [78]. This analogy shows that the required scale, while ambitious, is not unreasonable.

Selecting a high-emissivity material of $\epsilon = 0.9$ for the outer surface with a radius of $r = 78$ m yields an optimized electrical power output of $W_{\text{gen}} \approx 147$ MW. This corresponds to an annual electricity generation of roughly 1.29×10^3 GW h, which is sufficient to continuously power a population of approximately 429 thousand households [79].

Applying the 63% combined component efficiency derived in Sec. 6 to the idealized estimate yields a net electrical power output of 92.6 MW.

9.2 Design II: Buckyball Geodesic Frame

We now consider a Buckyball geodesic frame of radius r assembled from hexagonal and pentagonal steel panels. A Buckyball geodesic frame is far less susceptible to localized failure than a solid spherical shell due to its ability to redistribute loads through a redundant network of axial-force-dominated struts, thereby dissipating energy locally and resisting catastrophic buckling even under geometric imperfections. Suppose each steel panel is made of high-quality armor steel with side length $a = 7.5\,\mathrm{m}$ and thickness $H = 1.00\,\mathrm{m}$. Adjacent panels are joined along their edges by steel bars of cross-section $S = 1.00\,\mathrm{m}^2$.

The pressures imposed on the inner surface of the reactor are, respectively, $2.11 \times 10^6\,\mathrm{Pa}$ for neutrons and $1.32 \times 10^5\,\mathrm{Pa}$ for helium, again far less than the shear yield strength of the steel.

To estimate the maximum tensile mechanical force that the steel bars must withstand, we again employ a great-circle cut. The cut intersects approximately $\frac{2\pi r}{a}$ panel edges, each reinforced by one steel bar. The total area of the cross section resisting separation is therefore $\frac{2\pi r S}{a}$. Assuming all bars reach their tensile simultaneously, taking the yield in Eq. (30), the maximum force that the bars can sustain is

$$F_{\mathrm{max},2} = \frac{2\pi r S \sigma_{\mathrm{steel}}}{a} = r \cdot 1.34 \times 10^9\,\mathrm{Pa\,m}. \tag{33}$$

The tensile mechanical force imposed on the blanket by the neutron pulse was derived as in Eq. (28). The same requirement lead to

$$F_{\mathrm{n}}(r) \le F_{\mathrm{max},2}(r) \quad \Longrightarrow \quad r \ge 2.1 \times 10^2\,\mathrm{m}. \tag{34}$$

A sphere of this radius 210 m is comparable to an Iowa-class battleship with an overall length of 270 m [77].

With a high-emissivity material of $\epsilon = 0.9$ for the outer surface with a radius of $r = 210\,\mathrm{m}$ yields an electrical power output of $W_{\mathrm{gen}} \approx 1.06\,\mathrm{GW}$. This corresponds to an annual electricity generation of roughly $9.33 \times 10^3\,\mathrm{GW\,h}$, which is approximately 1/9

Table 3: System-level estimates for the two skeleton designs. Masses follow from the layer thicknesses and densities of Sec. 6. Fuel figures follow from Eq. (12) and the event frequency set by Eq. (15).

Quantity	Design I ($r = 78\,\mathrm{m}$)	Design II ($r = 210\,\mathrm{m}$)
Steel skeleton mass	$\sim 5.96 \times 10^5\,\mathrm{t}$	$\sim 4.56 \times 10^6\,\mathrm{t}$
Water and breeder mass	$\sim 7.65 \times 10^4\,\mathrm{t}$	$\sim 5.55 \times 10^5\,\mathrm{t}$
Tungsten armor mass	$\sim 1.48 \times 10^4\,\mathrm{t}$	$\sim 1.13 \times 10^4\,\mathrm{t}$
Event frequency	$\sim 0.5\,\mathrm{h}^{-1}$	$\sim 3.75\,\mathrm{h}^{-1}$
Tritium consumption	$\sim 32.5\,\mathrm{kg\,yr}^{-1}$	$\sim 243.4\,\mathrm{kg\,yr}^{-1}$
Tritium breeding	$\sim 40.9\,\mathrm{kg\,yr}^{-1}$	$\sim 306.5\,\mathrm{kg\,yr}^{-1}$
Pulses over 30 yr	$\sim 1.31 \times 10^5$	$\sim 9.85 \times 10^5$

of the annual electricity output of the Three Gorges Dam [80] and 1/20 of the annual electricity consumption of Shanghai [81].

Applying the 63% combined component efficiency derived in Sec. 6 to the idealized estimate yields a net electrical power output of 668 MW. The conclusion that the station operates in the gigawatt class remains unchanged.

10 System-level engineering estimates

We summarize the order-of-magnitude estimates for the principal engineering constraints. Derived directly from the physical framework of the preceding sections, these values are intended to define the macroscopic design boundaries rather than serve as a comprehensive engineering proposal.

The masses in Table 3 are the dominant engineering challenge of the concept and the primary motivation for Design II: hexagonal and pentagonal panels of the Buckyball frame can be manufactured on Earth and assembled in orbit, whereas the monolithic shell would require in-space fabrication at unprecedented scale.

Each event consumes the tritium content of one device, approximately 7.41 g per event for $f_{\mathrm{fus}} = 1$. With the breeding ratio of TBR = 1.259, the reactor produces more tritium than it consumes, so the fuel cycle is self-sufficient and able to start future stations. Deuterium is stable and can be stockpiled.

Component lifetimes are governed by the armor ablation rate and the mechanical

fatigue and the radiation damage mentioned in Sec. 8. The replaceable panel architecture of Design II allows to periodically exchange the most exposed components.

From a safety perspective, the station eliminates the risks of runaway chain reactions and decay-heat accidents. The system is inherently subcritical. Fusion only occurs when a device is deliberately delivered to the cavity center. Consequently, the radiological hazards are restricted to bred tritium, which poses a lower risk than long-lived fission isotopes, and the neutron-activated structural materials, which includes tungsten, beryllium, and steel. Furthermore, the thick multi-layer blanket structure effectively absorbs the gamma and X-ray emissions of each pulse, ensuring the safety of adjacent orbital infrastructure. While the physical safety profile is robust, deploying such a system must adhere to international space law regarding nuclear materials, a complex regulatory landscape that warrants its own comprehensive analysis.

11 Discussion

Our framework serves as a conceptual feasibility study for a space power station driven by pulsed and unconfined fusion, rather than a finalized engineering blueprint. While our analysis demonstrates that a sufficiently large structure can survive the mechanical and thermal loads of a single fusion event, transitioning from this conceptual design to an operational facility will require overcoming significant engineering challenges. For example, the in-orbit construction of such massive structures remains complex and costly. Furthermore, it is necessary to perform rigorous structural force modeling, detailed neutron transport simulations, comprehensive tritium cycle analyses, and irradiated material degradation evaluations. Beyond these considerations, practical designs for the cooling and power generation systems must also be developed alongside. These practical factors are currently either omitted or treated using simplified models in this paper, leaving them as critical avenues for future engineering research.

Fusion power stations based on pulsed and unconfined fusion reactions can be built both in space and on the ground. In this work, we focus on a space-based design for two

reasons. First, a weight-efficient power station is especially relevant to interstellar travel. Second, the high vacuum of space suppresses blast waves, leading to higher efficiency, less structural damage, and a simpler analysis. Ground-based stations operating on the same principle could be analyzed in a similar way, albeit with greater complexity, possibly using a giant vacuum cavity. We leave such investigations for future work.

Fusion power stations based on pulsed and unconfined fusion events would require a stable supply of fusion devices optimized for energy generation. Decommissioned thermonuclear devices, which must be periodically retired because of the limited half-life of tritium, could serve as a possible early pathway for such systems. In the long term, however, priority should be given to the mass production of devices designed specifically for energy generation.

Furthermore, pulsed and unconfined fusion reactions currently achieve a much higher fuel burn efficiency than controlled fusion reactions [82–84]. The fusion products of D-T fusions are neutrons and helium. These neutrons are turned into tritium by tritium breeder such as lithium or into deuterium by neutron moderator such as water. The tritium is then collected and used for future fusion events, minimizing the residues released into the environment. Only a few heavy radioactive isotopes can be produced by neutron activation of structural materials in such a reactor [85]. Because tritium is far less hazardous than those heavy long-life radioactive isotopes, public concerns about radioactive contamination are greatly reduced [86, 87].

Compared to conventional magnetic confinement architectures, our architecture exhibits a different design philosophy. While magnetic confinement architectures dedicate significant efforts to the scientific difficulties of establishing, stabilizing, and sustaining a burning plasma over time, our approach bypasses the continuous confinement problem entirely. By enlarging the containment cavity, we reduce the impact of the fusion burst on the surrounding material to a tolerable level, rather than actively confining the plasma itself. Consequently, the physics challenges of magnetic confinement are traded for the engineering difficulty of constructing a sufficiently large and robust structure. Although our approach offers a viable alternative to the bottlenecks of continuous magnetic con-

finement, it simultaneously introduces its own challenges, including the management of extreme structural responses, radiation damage, tritium cycles, and energy extraction.

In our current estimation, the overall electrical power output is bottlenecked by the cooling power of the outer surface via blackbody radiation. Mitigating this limitation requires enhancing the heat rejection rate. This can be achieved through two pathways. First, the total radiating surface area can be expanded by increasing the radius r. However, enlarging the structure in the space poses significant challenges from an engineering perspective. Alternatively, the cooling power can be amplified by increasing the cold bath temperature. To maintain the Carnot efficiency, a hotter cold bath requires a hotter hot bath. To further increase beyond 773 K, one can switch the working fluid of heat engine from supercritical water [64] to more advanced thermal mediums, such as high-temperature noble gas mixtures [88], which represents the most physically viable trajectory for pushing space-based fusion generation deep into the gigawatt regime.

In the present design, the water of the combined moderator–breeder layer serves several functions at once: it moderates the fusion neutrons, cools the structure by absorbing the deposited energy, attenuates residual gamma and X rays, and, being pressurized above its critical point, directly acts as the working fluid of the heat engine. This multi-use of water is efficient, but it ties the hot-bath temperature to the practical limit of supercritical water, $T_{\mathrm{hot}} \approx 773\,\mathrm{K}$. When the working fluid is switched to a high-temperature noble-gas mixture, these functions are decoupled. Water or another suitable medium retains the moderation and blanket-cooling functions and transfers the absorbed heat through a heat exchanger to a closed Brayton cycle relying on the noble gas to drive the turbine. The waste heat is then rejected to space by the radiator at the correspondingly higher cold-bath temperature. The hot bath temperature can thus be raised to the range 1200 K, as demonstrated in [88], with the cold bath following the maximum-power condition $T_{\mathrm{cold}} = 0.75 T_{\mathrm{hot}}$ of Sec. 6. Since the power output scales as T_{cold}^4, raising the cycle temperature increases the power output at fixed radius rapidly, while leaving the neutronics and structural analyses unchanged.

These pulsed and unconfined fusion events in space radiate gamma rays, X-rays,

ions, and electrons [14]. High voltages and currents can be generated when gamma rays and X-rays strike metallic components. Ions and electrons captured by Earth's magnetosphere form artificial radiation belts. Both of these phenomena can endanger satellites in space [89, 90]. In our design, these radiations are intentionally attenuated and absorbed by multiple material layers of the fusion power station, simultaneously maximizing the generated energy and minimizing the impact on satellites.

The pulsed and unconfined fusion events are usually triggered by fission events. The β decays of these fission and fusion products produce a huge number of neutrinos. Moreover, the high-energy neutrons from fusion reactions can induce additional fission in fissile or fertile materials, and react with the trigger's fissile material and with the fission products from the primary fission explosion. These secondary reactions produce further radioactive nuclei, whose β decays also emit neutrinos. All these neutrinos can be detected and studied on Earth, including their flavor oscillations during propagation. Thus, our space power station will also serve as a new neutrino source for neutrino physics.

While the mechanical pressure of the debris is orders of magnitude lower than that of the neutrons, the energy deposition mechanism is different. High-energy neutrons have a long mean free path and deposit their momentum and energy deep into the bulk blanket structure. Conversely, the massive and charged debris particles have a short mean free path and the mechanical and thermal load of the debris pulse is absorbed by the armor layer. While the bulk structural pressure is dominated by neutrons, the debris pulse acts as a severe challenge to the armor layer from the engineering perspective.

It is worth noting that our estimates are consistent with previous nuclear experiments. A notable example is Operation Crossroads, conducted by the U.S. Navy at Bikini Atoll in July 1946 [91]. In the Able test, a 2.3×10^4 tTNT nuclear device was deployed in air to start a nuclear event whose yield is more than an order of magnitude greater than the 1.00×10^3 tTNT fusion event assumed in our analysis. The Japanese battleship Nagato was positioned 910 m from the hypocenter. The thickness of the turret armor of Nagato was 305 mm and the belt armor tapering from 100 mm to 305 mm. This is comparable to the 1.00 m thickness assumed in our designs. Declassified reports show that Nagato

suffered no significant structural damage. Notwithstanding the distinctions on the exact values, this historical experiment indicates that large steel structures can survive nearby 10^3 tTNT nuclear event at a distance of 10^2 m, which is a necessary condition for the space-based pulsed and unconfined fusion power station to be feasible.

While this analysis establishes the fundamental thermodynamic and structural bounds of a space fusion reactor, several critical aspects require further investigation. Future work should prioritize rigorous Monte Carlo neutron transport simulations incorporating energy-dependent cross sections within the full spherical geometry as is mentioned in Sec. 4. Concurrently, dynamic structural simulations are necessary to model stress-wave propagation, ablation, thermal shock, mechanical fatigue or cumulative radiation damage discussed in Sec. 8. Beyond these immediate simulations, future efforts must replace the simplified toy model for efficiency in Sec. 6 with component-level power-conversion and radiator designs, finalizing a comprehensive system study addressing the in-orbit assembly, logistics, and legal frameworks governing space-based nuclear operations.

References

[1] Arcas, B. A. y. *et al.* Towards a future space-based, highly scalable ai infrastructure system design (2025). `2511.19468`.

[2] Duan, B. *et al.* On the innovation, design, construction, and experiments of omega-based ssps prototype: The sun-chasing project. *Engineering* **36**, 90–101 (2024). URL `https://www.sciencedirect.com/science/article/pii/S2095809923004733`.

[3] Jia, F. Space solar power station 'Zhuri project' research achieves breakthrough [空间太阳能电站"逐日工程"研究取得突破]. *People's Daily [人民日报]* 10 (2026). (in Chinese).

[4] Deutsch, C. & Tahir, N. A. Fusion reactions and matter–antimatter annihilation for space propulsion. *Laser and Particle Beams* **24**, 605–616 (2006).

[5] Barbarino, M. What is nuclear fusion? (2023). URL `https://www.iaea.org/newscenter/news/what-is-nuclear-fusion`. Accessed: 2026-02-13.

[6] Van Oost, Guido. *Fundamentals of magnetic fusion technology* (International Atomic Energy Agency (IAEA), 2023), 1st edn.

[7] a Method of Propulsion of Projectiles by Means of External Nuclear Explosions. Part 1, O. *Everett, C.J. and Ulam, S.M.* (Defense Technical Information Center, 1955), reprint edition edn.

[8] Schmidt, G., Bonometti, J. & Morton, P. Nuclear pulse propulsion-orion and beyond. In *36th AIAA/ASME/SAE/ASEE Joint Propulsion Conference and Exhibit*, 3856 (2000).

[9] Dyson, G. *Project Orion: The True Story of the Atomic Spaceship* (Henry Holt and Company, 2002), illustrated edn.

[10] Roth, J., Rayle, W. & Reinmann, J. *Technological Problems Anticipated in the Application of Fusion Reactors to Space Propulsion and Power Generation.* NASA technical memorandum (National Aeronautics and Space Administration, 1970).

[11] Williams, C. H. Nuclear fusion space propulsion research, experimentation, and analysis effort led by the nasa glenn research center (1996-2004). In *ASCEND 2020*, 4084 (2020).

[12] Romanelli, F. & Bruno, C. Assessment of open magnetic fusion for space propulsion. In *57th International Astronautical Congress*, C4–6 (2012).

[13] Razin, Y. S. *et al.* A direct fusion drive for rocket propulsion. *Acta Astronautica* **105**, 145–155 (2014).

[14] Glasstone, S., Dolan, P., of Defense, U. S. D. & of Energy, U. S. D. *The Effects of Nuclear Weapons* (U.S. Department of Defense, 1977).

[15] National Academy of Engineering and National Academies of Sciences Engineering and Medicine. *Bringing Fusion to the U.S. Grid* (The National Academies Press, Washington, DC, 2021).

[16] Lawson, J. D. Some criteria for a power producing thermonuclear reactor. *Proceedings of the Physical Society. Section B* **70**, 6 (1957).

[17] Linke, J. *et al.* Challenges for plasma-facing components in nuclear fusion. *Matter and Radiation at Extremes* **4**, 056201 (2019).

[18] Wesson, J. & Campbell, D. *Tokamaks*. International series of monographs on physics (Clarendon Press, 2004).

[19] Zhou, Y.-H., Park, D. & Iwasa, Y. Review of progress and challenges of key mechanical issues in high-field superconducting magnets. *National Science Review* **10**, nwad001 (2023).

[20] Kikuchi, M. & Azumi, M. Steady-state tokamak research: Core physics. *Rev. Mod. Phys.* **84**, 1807–1854 (2012).

[21] Breizman, B. N., Aleynikov, P., Hollmann, E. M. & Lehnen, M. Physics of runaway electrons in tokamaks. *Nuclear Fusion* **59**, 083001 (2019).

[22] Atzeni, S. & Meyer-ter Vehn, J. *The Physics of Inertial Fusion: BeamPlasma Interaction, Hydrodynamics, Hot Dense Matter* (Oxford University Press, 2004).

[23] Hurricane, O. A. *et al.* Physics principles of inertial confinement fusion and u.s. program overview. *Rev. Mod. Phys.* **95**, 025005 (2023).

[24] Kaplan, F. M. Enhanced-radiation weapons. *Scientific American* **238**, 44–51 (1978). URL `http://www.jstor.org/stable/24955730`.

[25] Abrams, M. Dawn of the e-bomb. *IEEE Spectrum* **40**, 24–30 (2003).

[26] Metzler, F., Hunt, C., Hagelstein, P. L. & Galvanetto, N. Known mechanisms that increase nuclear fusion rates in the solid state. *New Journal of Physics* **26**, 101202 (2024). URL `https://doi.org/10.1088/1367-2630/ad091c`.

[27] Chen, K.-Y. *et al.* Electrochemical loading enhances deuterium fusion rates in a metal target. *Nature* **644**, 640–645 (2025).

[28] Czerski, K. Deuteron-deuteron nuclear reactions at extremely low energies. *Phys. Rev. C* **106**, L011601 (2022). URL `https://link.aps.org/doi/10.1103/PhysRevC.106.L011601`.

[29] Dodaro, J. F. *et al.* Approach for fusion rate amplification through plasmonic resonance in closely-packed nanospheres. *Fusion Science and Technology* **0**, 1–8 (2026). URL `https://doi.org/10.1080/15361055.2026.2688026`. `https://doi.org/10.1080/15361055.2026.2688026`.

[30] Dyson, F. J. Search for artificial stellar sources of infrared radiation. *Science* **131**, 1667–1668 (1960).

[31] Long, F. A. Peaceful nuclear explosions. *Bulletin of the Atomic Scientists* **32**, 18–28 (1976).

[32] Hammond, R., Dooley, J. & Hubbard, H. Practical fusion power. *Mech. Eng.* **104**, 34–43 (1982).

[33] Moir, R. W. Pacer revisited*. *Fusion Technology* **15**, 1114–1118 (1989).

[34] Howarth, T. Nukes in space: Why a very very stupid idea just became more likely. *BBC Science Focus* (2024).

[35] Zheng, S.-T. The neutron bomb and its physics. *Physics* **30** (2001). URL `https://wuli.iphy.ac.cn/cn/article/id/30017`.

[36] Dobran, F. *Fusion Energy Harnessing, Reactor Technology, and Sustainability*, 1–69 (John Wiley & Sons, Ltd, 2017).

[37] Bosch, H.-S. & Hale, G. Improved formulas for fusion cross-sections and thermal reactivities. *Nuclear Fusion* **32**, 611 (1992).

[38] Laboratory, B. N. Evaluated nuclear data file (2024). URL `https://www.nndc.bnl.gov/endf/`. Accessed: 2026-01-23.

[39] Lucas, L. L. & Unterweger, M. P. Comprehensive review and critical evaluation of the half-life of tritium. *Journal of research of the National Institute of Standards and Technology* **105**, 541 (2000).

[40] Coc, A., Descouvemont, P., Olive, K. A., Uzan, J.-P. & Vangioni, E. Variation of fundamental constants and the role of a=5 and a=8 nuclei on primordial nucleosynthesis. *Phys. Rev. D* **86**, 043529 (2012).

[41] Koidan, V. *et al.* Effects of plasma interaction with radiation damaged tungsten. In *23rd IAEA Fusion Energy Conference*, p. 399 (2010). URL `https://inis.iaea.org/records/zv9k2-d5047`.

[42] Ziegler, J. F., Ziegler, M. & Biersack, J. Srim — the stopping and range of ions in matter (2010). *Nuclear Instruments and Methods in Physics Research Section B: Beam Interactions with Materials and Atoms* **268**, 1818–1823 (2010). 19th International Conference on Ion Beam Analysis.

[43] Cacuci, D. *Handbook of Nuclear Engineering: Vol. 1: Nuclear Engineering Fundamentals; Vol. 2: Reactor Design; Vol. 3: Reactor Analysis; Vol. 4: Reactors of Generations III and IV; Vol. 5: Fuel Cycles, Decommissioning, Waste Disposal and Safeguards*. No. v. 1 in Handbook of Nuclear Engineering (Springer, 2010).

[44] Mohanakrishnan, P., Singh, O. & Umasankari, K. *Physics of Nuclear Reactors* (Elsevier Science, 2021).

[45] Berger, M., Coursey, J., Zucker, M. & Chang, J. Stopping-power & range tables for electrons, protons, and helium ions. 2017. *NIST Standard Reference Database* **124** (2017).

[46] Duggal, V. P., Puri, S. M. & Ram, K. S. Attenuation of 14-mev neutrons in water and in 6-in. lead and water. *Nuclear Science and Engineering* **5**, 199–200 (1959).

[47] Hubbell, J. & Seltzer, S. Tables of x-ray mass attenuation coefficients and mass energy-absorption coefficients. *NIST Standard Reference Database* **126** (2024).

[48] Nogami, S. *et al.* Neutron irradiation tolerance of potassium-doped and rhenium-alloyed tungsten. *Journal of Nuclear Materials* **553**, 153009 (2021).

[49] Wang, Z. *et al.* Effect of rhenium on defects evolution behavior in tungsten under irradiation. *Nuclear Fusion* **61**, 036037 (2021). URL 10.1088/1741-4326/abd920.

[50] Hernández, F. & Pereslavtsev, P. First principles review of options for tritium breeder and neutron multiplier materials for breeding blankets in fusion reactors. *Fusion Engineering and Design* **137**, 243–256 (2018). URL https://www.sciencedirect.com/science/article/pii/S0920379618306392.

[51] Rubel, M. Fusion neutrons: tritium breeding and impact on wall materials and components of diagnostic systems. *Journal of Fusion Energy* **38**, 315–329 (2019).

[52] Billone, M., Donne, M. & Macaulay-Newcombe, R. Status of beryllium development for fusion applications. *Fusion Engineering and Design* **27**, 179–190 (1995). Proceedings of the Third International Symposium on Fusion Nuclear Technology.

[53] Wang, T. *et al.* A review on irradiated beryllium and beryllium alloy for fusion reactor application: Microstructure evolution, properties changes, and fabrication. *Fusion Engineering and Design* **211**, 114780 (2025).

[54] Piet, S., Jeppson, D., Muhlestein, L., Kazimi, M. & Corradini, M. Liquid metal chemical reaction safety in fusion facilities. *Fusion Engineering and Design* **5**, 273–298 (1987). URL https://www.sciencedirect.com/science/article/pii/S0920379687900329.

[55] Deoghar, A. *et al.* Development of lead lithium (pb-16li) alloy production system and characterization of the produced alloy. *Fusion Engineering and Design* **198**, 114072 (2024). URL https://www.sciencedirect.com/science/article/pii/S092037962300652X.

[56] Chapline, G., Hagmann, C., Kerr, P., Snyderman, N. J. & Wurtz, R. Cosmic ray induced neutron and gamma-ray bursts in a lead pile. Tech. Rep., Lawrence Livermore National Laboratory (LLNL), Livermore, CA (2007).

[57] Horný, V. c. v., Chen, S. N., Davoine, X., Gremillet, L. & Fuchs, J. Quantitative feasibility study of sequential neutron captures using intense lasers. *Phys. Rev. C* **109**, 025802 (2024).

[58] Cao, H. & Koltick, D. Cosmic ray induced neutron production in a lead target underground. *Astroparticle Physics* **178**, 103227 (2026).

[59] Abdou, M. *et al.* Blanket/first wall challenges and required r & d on the pathway to demo. *Fusion Engineering and Design* **100**, 2–43 (2015). URL `https://www.sciencedirect.com/science/article/pii/S0920379615302465`.

[60] Pint, B. A. The fusion liquid breeder compatibility gap: Thoughts on issues to address for a fusion power plant. *Current Opinion in Solid State and Materials Science* **41**, 101253 (2026). URL `https://www.sciencedirect.com/science/article/pii/S1359028625000403`.

[61] Zhang, C. *et al.* A study of the suppression of the high-temperature helium embrittlement in an oxide-particle dispersion strengthened alloy. *Chinese Science Bulletin* **53**, 3416–3421 (2008).

[62] Rieth, M. *et al.* Fabrication routes for advanced first wall design alternatives. *Nuclear Fusion* **61**, 116067 (2021).

[63] Steiner, D., Varsamis, G., Deutsch, L., Rathke, J. & Gierszewski, P. An aqueous lithium salt blanket option for fusion power reactors. *Fusion Engineering and Design* **8**, 207–212 (1989). URL `https://www.sciencedirect.com/science/article/pii/S0920379689801085`.

[64] Yoshiaki Oka, H. M. *Supercritical-Pressure Light Water Cooled Reactors* (Springer, Tokyo, 2014).

[65] Kerrebrock, J. L. Optimization of heat rejection in space. *Journal of Propulsion and Power* **2**, 562–563 (1986). URL https://doi.org/10.2514/3.22942. https://doi.org/10.2514/3.22942.

[66] Curzon, F. L. & Ahlborn, B. Efficiency of a carnot engine at maximum power output. *American Journal of Physics* **43**, 22–24 (1975). URL https://doi.org/10.1119/1.10023. https://pubs.aip.org/aapt/ajp/article-pdf/43/1/22/12091578/22_1_online.pdf.

[67] Mason, L. S. A power conversion concept for the jupiter icy moons orbiter. *Journal of Propulsion and Power* **20**, 902–910 (2004). URL https://doi.org/10.2514/1.5805. https://doi.org/10.2514/1.5805.

[68] Brolley, J. *et al.* A gas cerenkov detector for measuring 16.7 mev gamma rays from the d(t,γ)5he reaction. In *Los Alamos Conference on Optics 83*, vol. 380, 256–260 (SPIE, 1983).

[69] Ye, L.-R. & Lv, M. Physical problems in nuclear explosion and nuclear diagnosis. *Physics* **20** (1991). URL https://wuli.iphy.ac.cn/cn/article/id/28858.

[70] Bohachevsky, I. O. Scaling of reactor cavity wall loads and stresses. *Los Alamos Scientific Laboratory Report LA-7014-MS* (1979).

[71] Meier, W. R. *et al.* Osiris and SOMBRERO inertial confinement fusion power plant designs. Tech. Rep. WJSA-92-01, W.J. Schafer Associates, Inc. (1992).

[72] Kinsler, L. E., Frey, A. R., Coppens, A. B. & Sanders, J. V. *Fundamentals of Acoustics* (John Wiley & Sons, New York, 2000), 4th edn. URL https://books.google.com.hk/books?id=FecSEAAAQBAJ.

[73] Haynes, W. M. *CRC Handbook of Chemistry and Physics* (CRC Press, Boca Raton, 2016). URL https://books.google.com.hk/books?id=VVezDAAAQBAJ.

[74] Bergman, T. L., Lavine, A. S., Incropera, F. P. & Dewitt, D. P. *Fundamentals of Heat and Mass Transfer* (John Wiley & Sons, New York, 2011). URL https://books.google.com.hk/books?id=vvyIoXEywMoC.

[75] Troev, T., Angelov, V., Peneva, S. & Semkova, V. Displacement of atoms in fusion neutron irradiated fe and w. *Proceedings of the Bulgarian Academy of Sciences* **78**, 663–669 (2025). URL https://www.proceedings.bas.bg/index.php/cr/article/view/758.

[76] Bogusz, P., Nasiłowska, B. & Sławiński, G. Optical strain measurement and microfractography of the fractures of armstal 550 steel after temperature tensile tests. *Materials* **15** (2022). URL https://www.mdpi.com/1996-1944/15/24/8875.

[77] Sumrall, R. *Iowa Class Battleships: Their Design Weapons & Equipment* (Naval Institute Press, 1988).

[78] Wikipedia contributors. Sphere (venue) — Wikipedia, the free encyclopedia (2026). URL https://en.wikipedia.org/w/index.php?title=Sphere_(venue)&oldid=1352529520. [Online; accessed 5-May-2026].

[79] National Development and Reform Commission. Annual electricity consumption tops 10 trillion kwh for the first time, showcasing the vitality of china's economic development (2026). URL https://www.ndrc.gov.cn/wsdwhfz/202602/t20260204_1403586.html. Accessed: 2026-10-13.

[80] Wikipedia contributors. Three gorges dam — Wikipedia, the free encyclopedia (2025). URL https://en.wikipedia.org/w/index.php?title=Three_Gorges_Dam&oldid=1278511219. [Online; accessed 4-March-2025].

[81] Shanghai Economy and IT Committee. Shanghai electric power supply environmental sustainability key performance indicators report (2023). URL https://www.shanghai.gov.cn/gwk/search/content/8cd8e51540534c908c2d69565bf41c63.

[82] Brueckner, K. A. Theory And Experiment In Laser Driven Fusion. In Wuerker, R. F. (ed.) *Developments in Laser Technology II*, vol. 0041, 5 – 12. International Society for Optics and Photonics (SPIE, 1974).

[83] Tanabe, T. Tritium fuel cycle in iter and demo: Issues in handling large amount of fuel. *Journal of Nuclear Materials* **438**, S19–S26 (2013). Proceedings of the 20th International Conference on Plasma-Surface Interactions in Controlled Fusion Devices.

[84] Lan, K., Qiao, X., Li, Y., Zhao, X. & Sui, Z. Amplifier scheme for inertial confinement fusion: Principle, characteristics, and criteria. *Physics of Plasmas* **32**, 082708 (2025).

[85] Rubel, M. Structure materials in fusion reactors: Issues related to tritium, radioactivity and radiation-induced effects. *Fusion Science and Technology* **57**, 474–482 (2010).

[86] Thomas, G. Health risks from radiation–fission versus fusion. *Journal of Fusion Energy* **42**, 20 (2023).

[87] Sartayev, Y. & Hayashida, N. Fukushima's tritiated water discharge: Health and environmental implications derived from historical nuclear incidents. *Journal of Environmental Radioactivity* **290**, 107814 (2025).

[88] El-Genk, M. S. & Tournier, J.-M. Noble-gas binary mixtures for closed-brayton-cycle space reactor power systems. *Journal of Propulsion and Power* **23**, 863–873 (2007). URL `https://doi.org/10.2514/1.27664`. `https://doi.org/10.2514/1.27664`.

[89] Hess, W. N. The artificial radiation belt made on july 9, 1962. *Journal of Geophysical Research* **68**, 667–683 (1963).

[90] Brown, W. L. & Gabbe, J. The electron distribution in the earth's radiation belts during july 1962 as measured by telstar. *Journal of Geophysical Research* **68**, 607–618 (1963).

[91] Wikipedia contributors. Operation crossroads — Wikipedia, the free encyclopedia (2026). URL https://en.wikipedia.org/w/index.php?title=Operation_Crossroads&oldid=1336912261. [Online; accessed 14-February-2026].